LAWRENCE
LIVERMORE
NATIONAL
LABORATORY

LLNL-TR-788566

FissionTPC FY2019 Report

L. A. Snyder

August 30, 2019

Disclaimer

This document was prepared as an account of work sponsored by an agency of the United States government. Neither the United States government nor Lawrence Livermore National Security, LLC, nor any of their employees makes any warranty, expressed or implied, or assumes any legal liability or responsibility for the accuracy, completeness, or usefulness of any information, apparatus, product, or process disclosed, or represents that its use would not infringe privately owned rights. Reference herein to any specific commercial product, process, or service by trade name, trademark, manufacturer, or otherwise does not necessarily constitute or imply its endorsement, recommendation, or favoring by the United States government or Lawrence Livermore National Security, LLC. The views and opinions of authors expressed herein do not necessarily state or reflect those of the United States government or Lawrence Livermore National Security, LLC, and shall not be used for advertising or product endorsement purposes.

This work performed under the auspices of the U.S. Department of Energy by Lawrence Livermore National Laboratory under Contract DE-AC52-07NA27344.

FissionTPC FY2019 Report: Preliminary $^{235}U(n,f)/^{6}Li(n,t)\alpha$ Cross Section Ratio Data & Update on the $^{239}Pu(n,f)/^{235}U(n,f)$ Cross Section Ratio

The NIFFTE Collaboration

Lawrence Livermore National Laboratory
Los Alamos National Laboratory
Abilene Christian University
Oregon State University
California Polytechnic State University San Luis Obispo
Colorado School of Mines

LLNL-TR-788566

Sept. 13, 2019

This work was performed under the auspices of the U.S. Department of Energy by Lawrence Livermore National Laboratory under contract DEJAC52J07NA27344. Lawrence Livermore National Security, LLC.

Summary

The primary motivation for the fissionTPC experiment is to provide precise, accurate data for evaluation of the ^{239}Pu(n,f) cross section. Neutron induced fission cross sections are typically measured as ratios, with a well known standard cross section being in the denominator. Measuring a ratio removes the need to quantify the neutron beam flux which is difficult to determine accurately. Any cross section ratio measurement is ultimately limited by the accuracy of the standard used. While the ^{235}U(n,f) standard is well measured some light particle reactions are known as well or better. Light particle reactions also remove some of the shared systematic uncertainties that are present in an actinide-only ratio measurement. To this end the NIFFTE collaboration originally proposed to measure the ^{239}Pu(n,f)/^{1}H(n,el) cross section ratio. The ^{1}H(n,el) reaction is well measured, smoothly varying as a function of energy and has good theoretical support, making it an ideal candidate for a cross section standard. Through simulation-based study and initial data collection with the fissionTPC of a ^{235}U(n,f)/^{1}H(n,el) cross section ratio it was determined that the measurement uncertainties could not be reduced sufficently to take full advantage of the high accuracy of the ^{1}H(n,el) reaction. The primary difficulties faced were the low energy of the scattered protons which do not provide enough signal to measure the neutron time-of-flight (nToF) with the fissionTPC fast cathode amplifier, and the the background (n,p) signals induced by the high energy component of the WNR beam. It should be noted that these challenges would be greatly reduced if we were to make such a measurement at a monoenergetic neutron facility.

In light of these challenges other reactions were investigated. The ^{6}Li(n,t)α reaction was identified as a good alternative. The 4.8 MeV Q-value of the reaction provides a relatively large signal for nToF determination and the two charged particles (t & α) released in the reaction provide a signal well suited for background suppression in the fissionTPC. The ^{6}Li(n,t) reaction is considered a standard up to 1 MeV and is currently evaluated up to 3 MeV incident neutron energy. While this is a narrower energy range than the ^{1}H(n,el) reaction it overlaps well with the fission neutron spectrum. A mock evaluation was performed and it was estimated that a measurement of ^{239}Pu(n,f)/^{6}Li(n,t) would have an impact on the ^{239}Pu(n,f) evaluation comparable to a measurement using a the ^{1}H(n,el) reaction. While the ^{6}Li(n,t) reaction is not as well measured as the ^{1}H(n,el) reaction, the lack of previous measurements in the GMA database means that a new measurement of ^{239}Pu(n,f)/^{6}Li(n,t) will have a greater weighting and therefore a large impact on a future evaluation. In addition to providing a reduction in the ^{239}Pu(n,f) cross section evaluation uncertainties, a measurement of ^{6}Li(n,t) in the fissionTPC will provide data to resolve a discrepancy in previous measurements of the reaction above 1 MeV. Furthermore, the ^{6}Li data collected in the fissionTPC can also be analyzed to measure the ^{6}Li(n,nd) reaction for which there is limited discrepant data in the GMA database.

This report will focus on: the motivation for making a ^{239}Pu(n,f)/^{6}Li(n,t) cross section ratio measurement; a preliminary look at ^{235}U(n,f)/^{6}Li(n,t) data collected which will emphasize the capability of the fissionTPC to make an nToF measurement with the fast cathode amplifier; and finally will provide a brief update on the ^{239}Pu(n,f)/^{235}U(n,f) cross section analysis.

Contents

1 Introduction **3**

2 Measuring the ^{6}Li(n,t)α Reaction in the fissionTPC **8**
2.1 Efficiency . . . 8
2.2 Preliminary Data . . . 9

3 Status of the ^{239}Pu(n,f)/^{235}U(n,f) Cross Section Measurement **12**
3.1 The Overlap Correction . . . 12
3.2 The Binned Analysis . . . 16
3.3 Cross Section Shape Validations and Sensitivity Studies . . . 18
3.3.1 Rotation . . . 18
3.3.2 Radius Cut . . . 19
3.3.3 Polar Angle, θ, Cut & Track Vertex Bias . . . 21
3.3.4 Target Alignment . . . 23
3.3.5 Space Charge Scaling . . . 23
3.3.6 Tracking Resolution . . . 24
3.4 Cross Section Normalization . . . 26
3.4.1 Summary . . . 28

1 Introduction

Nuclear data plays an important role in both defense and energy related applications. These systems have become increasingly dependent on advanced simulation and modeling. Ultimately the accuracy of these models are no better than the underlying uncertainties of the nuclear data they use. It is therefore imperative that nuclear data uncertainties are minimized and well-understood. Specifically, there is a need for precision neutron-induced fission cross section measurements on fissile nuclei such as ^{239}Pu.

The NIFFTE collaboration, comprised of two national laboratories and four universities, has developed the fissionTPC to measure energy-differential neutron-induced fission cross section ratios with total uncertainties less than 1% (both statistical and systematic). For comparison, traditional measurements using ionization chambers are limited to 3–5% total uncertainty.

The fissionTPC has several advantages over standard ionization chambers, most notably when it comes to providing insight into sources of systematic uncertainties. Charged particle tracks are reconstructed by combining the 2D information from the finely-segmented readout plane with the relative drift time of the track. This particle tracking information can help determine sample uniformity, beam profile, and other parameters which were often estimated rather than measured in previous measurements. In addition, it also enables improved discrimination of fission fragments, alphas and other charged particles (see Fig. 1). An extensive description of the fissionTPC can be found in Ref. [1].

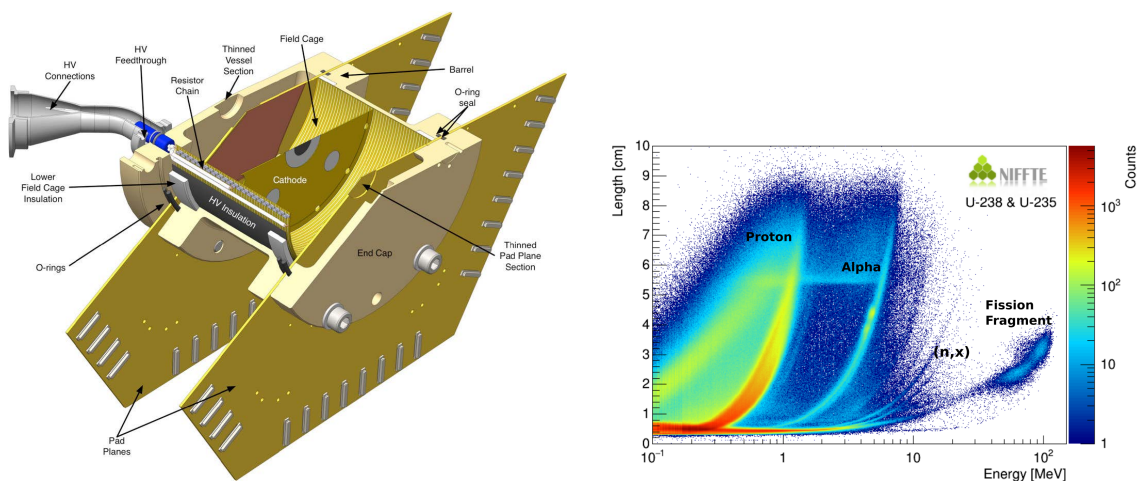

Figure 1: (Left) A cut-away of the fissionTPC detector. (Right) Reconstructed charged-particle track lengths and energies from fissionTPC data. Bands for various isotopes ranging from protons to fission fragments are visible.

The primary goal of the fissionTPC project is to measure the ^{239}Pu(n,f) cross section to sub-1% accuracy. More importantly the goal is to provide an accurate measurement with a detailed uncertainly analysis, including all the correlations, upload the information to the appropriate databases and in turn have an impact on the ^{239}Pu evaluation. Providing precision measurements requires extensive effort and a methodical approach. To this end the fissionTPC project has made a series of detector development and validation measurements. The 3 phases as originally planned were to:

1. Measure ^{238}U(n,f)/^{235}U(n,f) cross section ratio to benchmark the fissionTPC performance. The unnormalized data were published [2] and uploaded to the EXFOR and GMA databases.

2. Measure the ^{239}Pu(n,f)/^{235}U(n,f) cross section ratio. The preliminary result for this ratio has been released [3]. The effort to validate and normalize the results before publication continues [4].
3. Measure the ^{239}Pu(n,f)/^{1}H(n,el) cross section ratio. Data collection at LANSCE completed.

Ultimately the uncertainty of any cross section ratio measurement is limited by the uncertainty of the reference standard. The ^{1}H(n,el) cross section is the most accurate neutron standard. After significant development, simulation, data collection and analysis it was determined that the measurement uncertainties for ^{1}H(n,el) with the fissionTPC at LANSCE would be too great to effectively capitalize on the low uncertainty of the standard in an evaluation. This led to the exploration of other light-particle standards.

It was proposed to measure the ^{235}U(n,f)/^{6}Li(n,t)α cross section ratio as a precursor development measurement to a ^{239}Pu(n,f)/^{6}Li(n,t)α cross section ratio the following year. ^{6}Li(n,t)α has many advantages compared to ^{1}H(n,el) from a detection standpoint: solid, thin targets in the form of LiF can be made with relative ease; the large Q-value of 4.8 MeV provides sufficient energy for a fast cathode timing signal for nToF; and the two charged particles emitted in the reaction provide an excellent event tag and background suppression in a TPC. Taken together these advantages make sub-percent measurement uncertainties with the fissionTPC at LANSCE much more achievable than for a ^{1}H(n,el) measurement.

Crucially, we also performed a mock data evaluation to understand the impact of a ^{239}Pu(n,f)/^{6}Li(n,t)α measurement on a future ENDF evaluation and compared it to the potential impact of a ^{239}Pu(n,f)/^{1}H(n,el) measurement [5]. It was found that while the ^{6}Li based evaluation is possible over a narrower energy range of $\approx 0.15 - 3$ MeV, the reduction in uncertainties would be comparable and in some cases better than for a ^{1}H based measurement. Figure 2 shows the results of the mock evaluation of ^{239}Pu(n,f) with either ^{6}Li or ^{1}H standard. The figure shows the reduction in evaluation uncertainty that would be expected with the introduction of new data. The various colored lines represent different evaluations when altering assumptions about two key measurement uncertainties: the background (b) and the normalization (N).

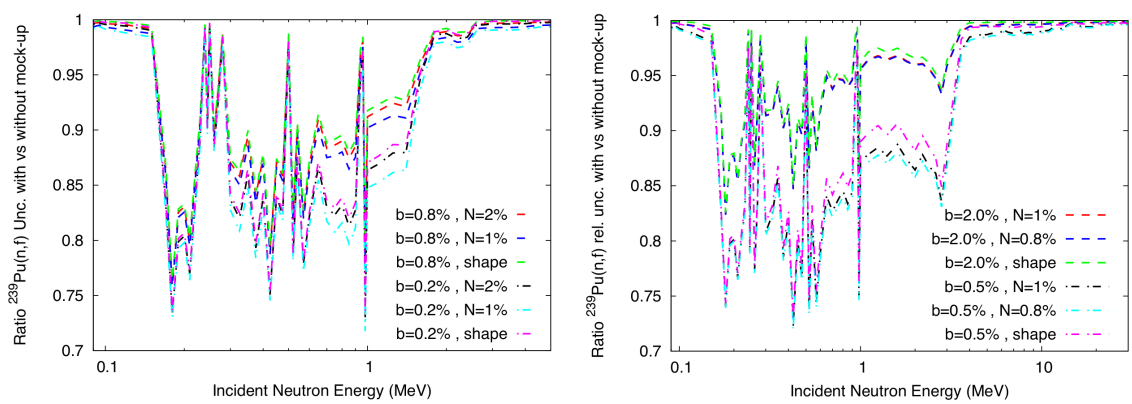

Figure 2: The change in evaluation uncertainty of ^{239}Pu(n,f) with new fissionTPC data from measurements in ratio to either the ^{6}Li(n,t)α standard (Left) or the ^{1}H(n,el) standard (Right). The vertical scale is the ratio of the evaluation uncertainty with the additional data to the uncertainty without the new data, where <1 is the fractional decrease in uncertainty and >1 would be an increase. The various colored lines represent different evaluations when altering assumptions about two key measurement uncertainties: the background (b) and the normalization (N).

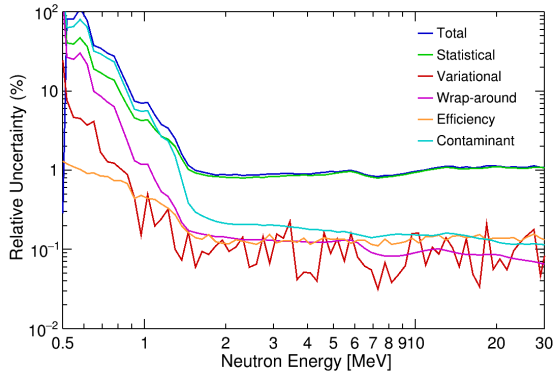

Figure 3: Measurement uncertainties from the fissionTPC measurement of the ^{238}U/^{235}U fission cross section ratio [2]. These uncertainties were used as the basis for the assumptions in the mock evaluations of ^{239}Pu/^{6}Li and ^{239}Pu/^{1}H cross section ratios shown in Figure 2.

The assumptions about measurement uncertainties are based on previous experience measuring ^{238}U/^{235}U fission cross section ratios [2] which can be seen in Figure 3. The background uncertainty was varied as it is expected to be one of the largest and has the least in common with our assumptions, which are based on an actinide-only ratio measurement. The correction for a light charged particle background will be considerably different than for a fission fragment background. The target atom number normalization will also have either a relatively large uncertainty or will not be feasible at all. This is a result of the fact that we can not use α-counting to determine the ^{6}LiF target mass. Other measurement techniques of target density and thickness are difficult in the context of the fissionTPC and will typically have uncertainties greater than 1% or not be possible at all. Figure 2 shows that even with a shape only measurement the reduction in evaluation uncertainties will still be considerable.

The uncertainties for a ^{239}Pu/^{6}Li measurement are comparable to a ^{239}Pu/^{1}H measurement of similar precision as a result of the lack of previous ^{239}Pu/^{6}Li measurements in that energy range reported in the GMA database [6]. With no other data points present a single measurement has a stronger weighting on the evaluation. It should be noted that our mock evaluation does not include the impact of "Unrecognized Systematic Uncertainties" (USU) [7]. These were not included as they are applied to an evaluation a-posterior and are not included in the standards database. Furthermore, it is our understanding that the USU formalism is planned to be revised [5] and a fissionTPC measurement could have an impact on that outcome.

Our mock evaluation also indicates that ratio measurements of ^{6}Li(n,t) with the fissionTPC will have a considerable impact on the ^{6}Li evaluation above 1 MeV. Figure 4 shows a comparison between ENDF and the 2017 Standards for ^{6}Li(n,t) cross section above 1 MeV and the anticipated reduction in uncertainties for that cross section resulting from our mock evaluation. The potential for such a considerable reduction in uncertainties is a result of discrepancies in the existing ^{6}Li(n,t) data. Figure 5 (taken from Ref. [7]) shows the overlay of the standards and some of the contributing data. One contributing factor to this disagreement is the result of an effect termed "particle leaking" which was noted by Giorginis et al. [8,9]. Particle leaking refers to a kinematic effect whereby, for certain outgoing angles of the triton, both the t and α products are emitted at forward angles. For detectors that cannot resolve the particles, this effect causes a misidentification of the products as a t + α composite particle with the sum of the individual energies. In turn, this can cause a systematic underestimation of the ^{6}Li(n,t) cross section. The fissionTPC is well suited to resolve this discrepancy as it has nearly 4π coverage and can distinguish particle types

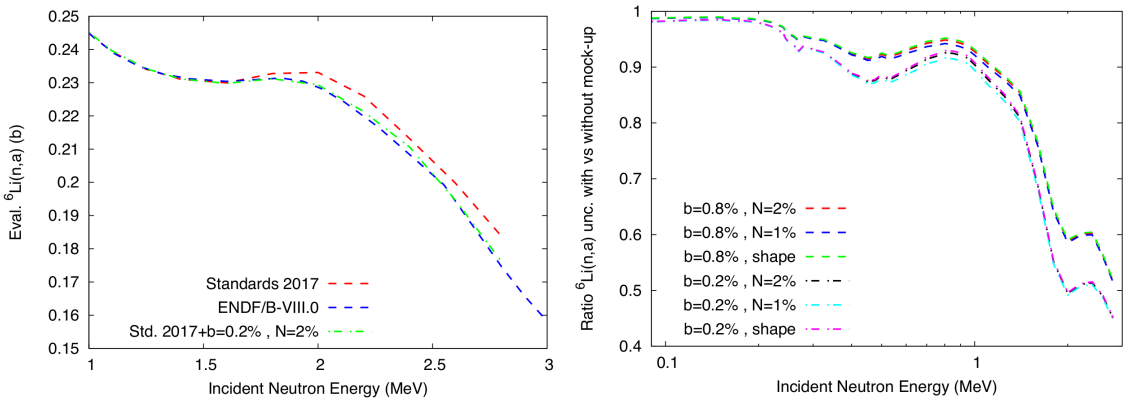

Figure 4: (Left)The evaluation of the ^{6}Li(n,t) reaction from ENDF and the 2017 Standards [7]. (Right) The decrease in the ^{6}Li(n,t) evaluation uncertainties based on our mock evaluation. The significant reduction is a result of our estimation that fissionTPC data will help address the discrepant data and evaluations.

in multi-particle reactions.

Another potential source of the data discrepancies is the ^{6}Li(n,nd)t break-up reaction. Figure 6 shows the evaluations of the various ^{6}Li+n reactions. As the (n,t) reaction begins to roll off at $\approx$ 2.5 MeV the (n,nd) reaction cross section rises steeply. Deuterons and tritons can be difficult to distinguish and one reaction could be attributed as the other leading to a systematic error. The particle distinguishing ability of the fissionTPC should be able to distinguish these reactions. While helping to improve the ^{6}Li(n,t) measurement above 1 MeV a measurement with the fissionTPC has the added benefit of contributing data to the ^{6}Li(n,nd) reaction. Figure 6 includes an overlay of the data included in the ^{6}Li(n,nd) evaluation. The dataset has large uncertainties, is discrepant below 7 MeV and limited above that energy. A fissionTPC measurement at LANSCE could have a significant impact on the ^{6}Li(n,nd) evaluation.

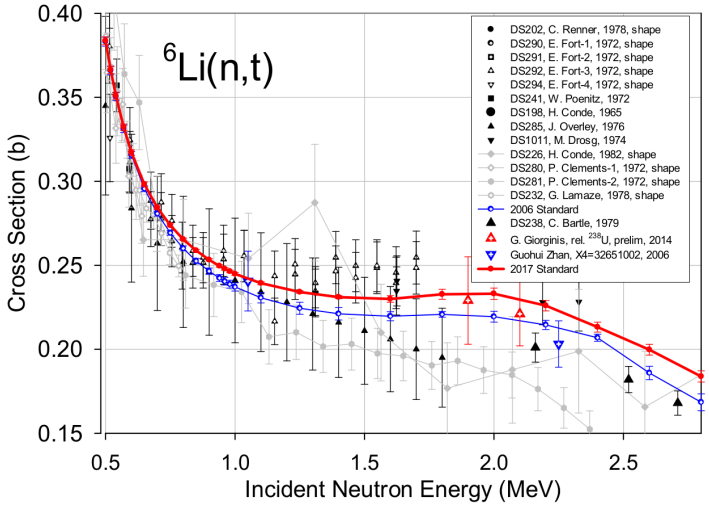

Figure 5: Figure taken from Reference [7]. The ^{6}Li(n,t) reaction is considered a standard up to 1 MeV. Above that energy the uncertainties increase and contributing data sets are discrepant.

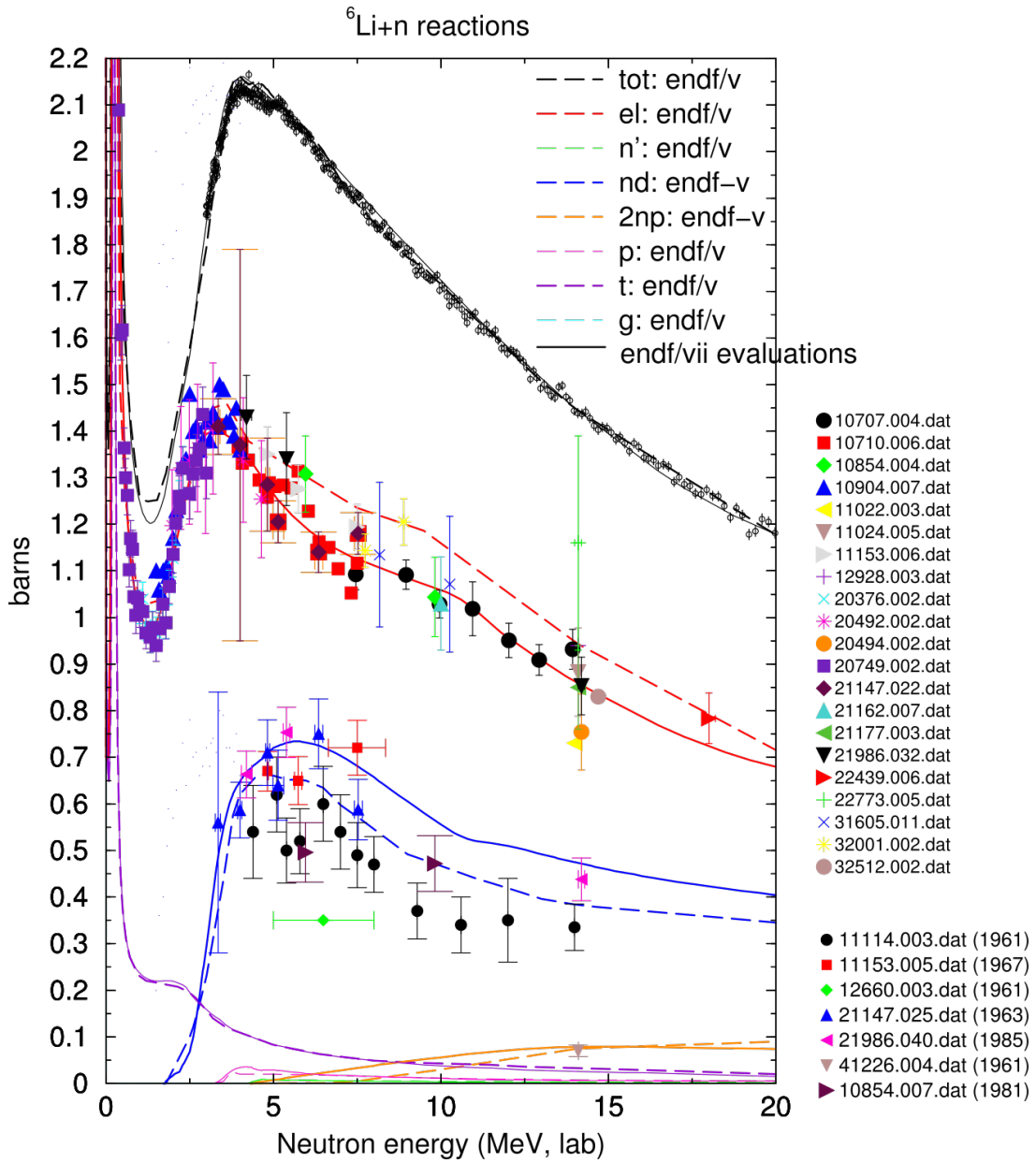

Figure 6: The evaluations of the various ^{6}Li+n reactions from ENDF/V and ENDF/VII. Data for the (n,nd) and (n,el) reactions are over-layed. Note that the (n,nd) reaction (blue) cross section is rising steeply as the (n,t) reaction (purple) is rolling off. The difficulty in distinguishing deuterons from tritons experimentally could contribute to the observed data discrepancies seen in Figure 5. A fissionTPC measurement of ^{6}Li(n,t) at LANSCE will also contribute data to the ^{6}Li(n,nd) cross section.

2 Measuring the ^{6}Li(n,t)α Reaction in the fissionTPC

2.1 Efficiency

The target for measuring the ^{235}U(n,f)/^{6}Li(n,t) consists of an approximately 0.4μm thick ^{6}LiF deposit and a 0.1 μm thick $^{235}UF_4$ deposit on a 1 μm thick aluminum backing. The Al foils were mounted on 0.5 mm thick target rings by the Lebow corporation. The ^{6}LiF was vapor deposited at LLNL and the $^{235}UF_4$ was vapor deposited at Oregon State University. The ^{235}U thickness was based on previous experience at LANSCE and the ^{6}Li thickness was set to match the expected statistical rate of the ^{235}U(n,f) at 5 MeV. The Al backing is transparent to alphas and tritons from ^{6}Li(n,t). Figure 7 shows an example of the energy-angle distribution of alphas and tritons, which are approximately back-to-back, though the kinematics of the reaction for non-thermal neutron energies means they are not precisely so. To take advantage of the two-particle background suppression both particles must be identified. Even with a thin backing there will be some angular ranges for which the tritons and/or alphas lose most or all of their energy outisde of the fissionTPC active volume. An efficiency correction is therefore required. Figure 8 shows the results of a SRIM simulation for the fraction of detectable energy that enters the gas volume of the fissionTPC. The efficiency corrections will be a modification of the current fissionTPC efficiency model which is described in Ref. [2]. The energy-loss/efficiency model takes into account the mass and charge of the emitted particle and the angular distribution resulting from anisotropy and kinematic boost.

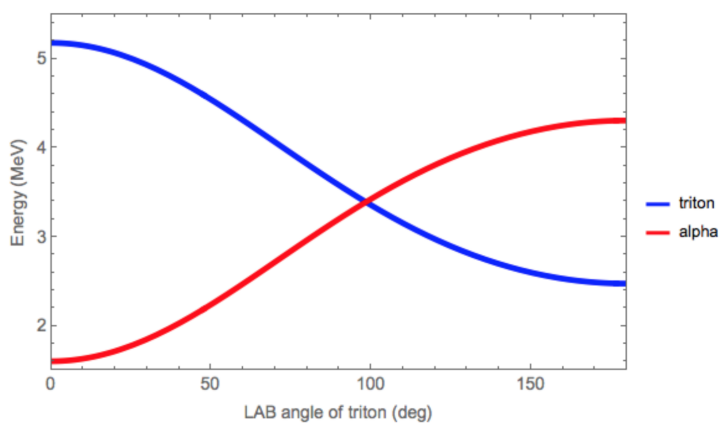

Figure 7: The energy vs. angle distribution for alphas and tritons emitted in the ^{6}Li(n,t)α reaction. This distribution is an example at an incident neutron energy of 2 MeV.

The primary difference between the detection of the fission fragments and the ^{6}Li reaction products is that the fission fragments are much more energetic. This has no implications for the detection efficiency of the particles on the anode, which has a gas gain stage. The fast cathode signal, which is used for the neutron time-of-flight determination, has no gas gain stage however. The long range and low energy density of the alpha and triton tracks will make them difficult to detect above the beam-induced background and signal noise, complicating the efficiency calculation. The gas mixture and pressure affect the energy density (range) of the charged particle tracks in the fissionTPC. Increasing the pressure decreases the track length and increases the charge density, thereby improving amplifier performance. Beam time will be required to fully study the optimum settings, particularly in the case of gas mixtures and pressure, as the ^{6}Li(n,t)α reaction cannot be replicated in the lab and the in-beam behavior of the MICROMEGAS gain stage is dependent on the gas type. Our previous efforts with fissionTPC development for the detection of ^{1}H(n,el)

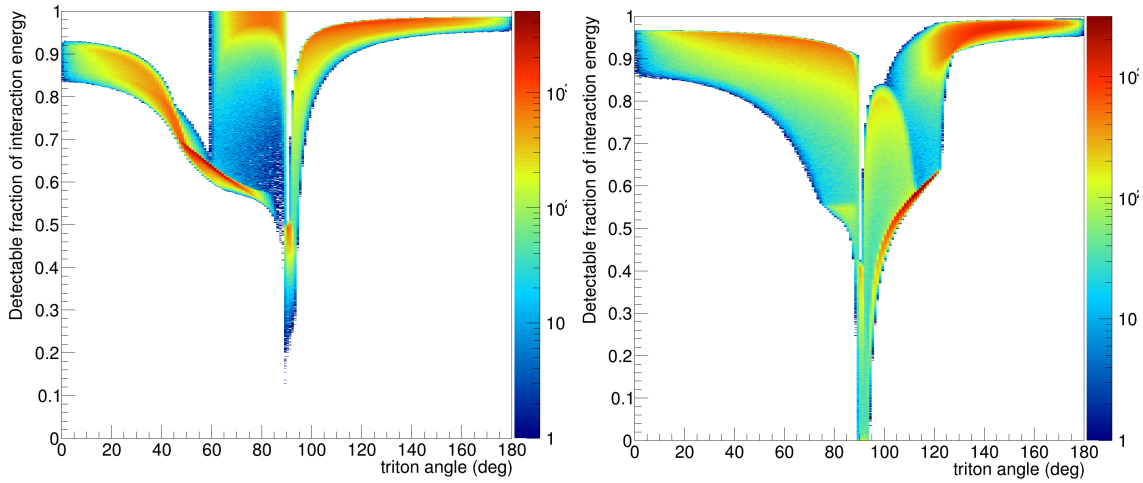

Figure 8: A simulation of the fraction of detectable energy in the fissionTPC after accounting for energy loss in the target and backing. The two plots represent two different orientations of the target and backing with respect to the beam. The triton preferentially travels in the direction of the neutron beam and is the more penetrating of the two particles. It is therefore optimal to orient the target backing downstream in the beam direction. The apparent discontinuities in the plots are a result of both particles traveling into the same volume of the detector.

reactions has been instructive. The amplifier was designed and gas studies [10] performed in anticipation of detecting low energy proton tracks. If the energy of at least one of the particles and the angles of both are known the reaction kinematics can be used to infer the incident neutron energy. There is a dependence on the $\sin^2\theta$ of the reaction however which will significantly limit the neutron energy resolution. This calculation is intended to only be used as a cross check for the nToF measurement but it could be relied upon in the case of severely limited cathode amplifier performance.

2.2 Preliminary Data

The ^{235}U(n,f)/^{6}Li(n,t) has been deployed in beam at LANSCE. Preliminary data is being used to explore the optimum operating conditions for the fissionTPC. These include adjustments to gas mixture, pressure and gain. The α tracks from the ^{6}Li reaction preferentially travel upstream of the beam direction and are of an energy range of 2–3 MeV (see figure 7). The target was placed such that the ^{6}Li deposit is upstream of the Al foil backing allowing the lower energy α tracks to be emitted without having to pass through the foil backing, while the much more penetrating tritons will predominately pass through the foil backing. Figure.... shows data and simulation for the two volumes (up and downstream) of the fissionTPC. Beam off data shows the spontaneous decay αs from the ^{235}U deposit. The αs have lost energy in the upstream volume after passing through the relatively thick 1 μm Al foil. The simulation shows the reaction products of the ^{6}Li(n,t)α reaction. The simulation in the downstream volume also includes some gas scatter proton tracks for illustrative purposes. The beam on data includes several particles not included in the simulation such as Argon gas recoils and fission fragments. When comparing the beam off, beam on and simulation data of the upstream volume in particular, the presence of the αs from the ^{6}Li reaction are distinctly visible. In the upstream simulation a region of particles referred to as "leaking" is also visible. These are ^{6}Li reactions where both the triton and α are at a shallow angle with respect to

each other and almost perpendicular to the beam. The opening angle is such that they both appear in the same volume as a single long track. Particle leakage was discussed in section 1 as a possible problem for previous measurements. The fissionTPC is well suited to identifying these events.

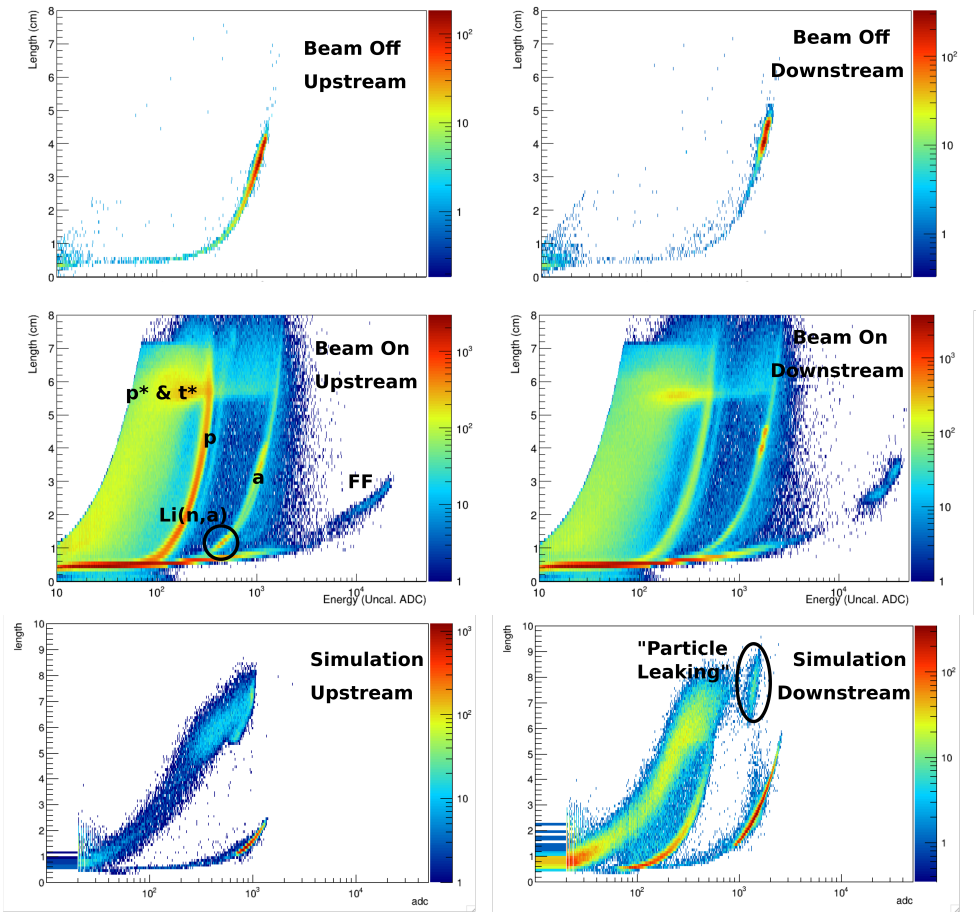

Figure 9: Track length vs. track energy fissionTPC data with the ^{235}U(n,f)/^{6}Li(n,t) target for both beam off and beam on. Also included is a simulation of the ^{6}Li(n,t)α reaction products. Upstream and downstream refer to the volume with respect to the neutron beam direction. The downstream simulation also includes beam induced proton scatters to clarify the position of the αs relative to the high energy tritons. The proton scatters are fully contained while the tritons and protons labeled p* & t* leave the active area of the detector and only deposit a fraction of their total energy. The αs from the ^{6}Li reaction are clearly visible in the upstream beam data.

Figure 10 shows to waveforms from the high-speed cathode signal that is used to reconstruct the nToF. The panel on the left shows the waveform associated with an ^{6}Lireaction. The panel on the right shows on for a fission event. The need for a wide dynamic range is clear, the fission event deposits over 10x as much energy on the cathode as that of the ^{6}Li reaction. The signal-to-noise ratio for the ^{6}Li reaction is sufficient to determine a nToF, however it is not clear that the cathode will be 100% efficient for detecting the ^{6}Li reaction products.

Preliminary ^{235}U(n,f)/^{6}Li(n,t) has been collected in beam at LANSCE. The ^{6}Li(n,t)α reaction products are clearly visible in the fissionTPC data. Initial analysis indicates that the high-speed cathode will be able to produce signals sufficienc to reconstruct nToF though further analysis is required to determine the efficiency of the cathode to detect ^{6}Li(n,t) reactions. Data collection and

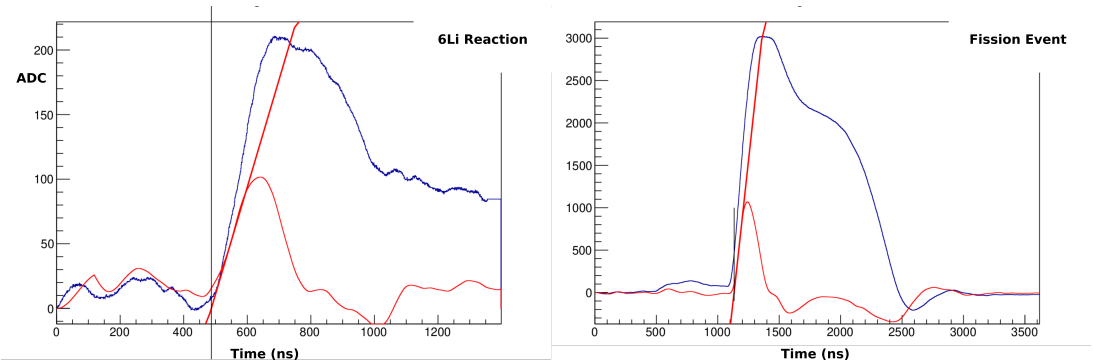

Figure 10: High-speed cathode waveforms for an ^{6}Lireaction (left) and a fission event (right). The fission event is over 10x the strength of the ^{6}Li signal. The ^{6}Li signal is sufficient for the determination of nToF.

analysis is ongoing to determine the optimum settings for the fissionTPC gas and gain.

3 Status of the ^{239}Pu(n,f)/^{235}U(n,f) Cross Section Measurement

As with any precision measurement careful validation of the results and rigorous quantification of the uncertainties is required. Our approach has been to make multiple experimental configuration changes and to use several analysis techniques to test both data correction models and detector performance.

The analysis focus to this point has been on a correction for beam and target nonuniformities and the fission fragment detection efficiency, which are both relatively complex and rely in part on modeling. The ability to directly measure inputs for the determination of these two corrections were motivations for developing the fissionTPC in the first place since past fission chamber measurements relied upon experimental design to minimize their impact. Using relatively simple fission chambers it is not possible to directly correct for these effects. The primary data validation used here is rotation of the fissionTPC with respect to the neutron beam direction. This configuration change has the largest possible impact on the efficiency and beam / target overlap. Two analysis techniques were employed in this work that use the tracking capabilities of the fissionTPC: a tracking based correction of the beam / target overlap and a binned vertex analysis that bypasses the beam / target overlap correction. While both methods rely on reconstruction of α-decay and fission fragment track vertices the methods for computing the final result are not mathematically equivalent. **The rotation validation and two analysis techniques are currently in agreement. These are the primary validations for the fissionTPC cross section measurement and the agreement indicates that we have successfully measured a cross section shape.** Some effort remains to validate the overall target normalization.

In the FY17 and FY18 [3,4] reports an MCNP-based correction of the beam / target overlap was used. It was determined that adding the additional step of an MCNP simulation in the analysis added no quantitative value to the result. It is however a useful qualitative validation of the beam nonuniformity. No significant changes were seen when using a data-only method for the overlap term as compared to an MCNP-based method.

The major finding in the FY18 report was that the so called *overlap correction* and *binned analysis* methods were not in agreement. This disagreement was traced to the method with which the efficiency correction was being applied to the binned analysis. The binned and overlap analyses used different fission fragment selection cuts. The efficiency correction must be adjusted for each cut selection. However, a single efficiency correction was being used for both analyses. We have adjusted the cut selections for the current analysis so that the same efficiency correction applies to both. A clerical error was also identified in which the incorrect target normalization was being applied. Efforts to perform an extensive internal audit of the analysis and uncertainty quantification are still ongoing.

3.1 The Overlap Correction

In a typical fission chamber measurement an attempt is made to place two actinide targets in the same neutron beam. When constructing a cross section ratio the neutron flux term then divides out and eliminates the need to measure it. This method still works if one of either the beam or targets has nonuniformities. When both the beam and a target have nonuniformities the cross section ratio must have an energy dependent normalization correction applied. It is the case for the fissionTPC data that the ^{239}Pu target and the beam were both nonuniform. An image depicting variation in the ^{239}Pu target thickness is shown in Fig. 11, and a Monte Carlo calculation (MCNP) of the neutron intensity, showing spatial nonunifomity, is shown in Figure 12.

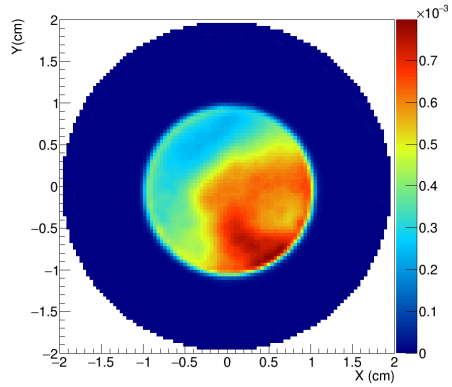

Figure 11: Spontaneous α-decay track start vertices for the ^{239}Pu target. The rate of α-decay is proportional to the target thickness.

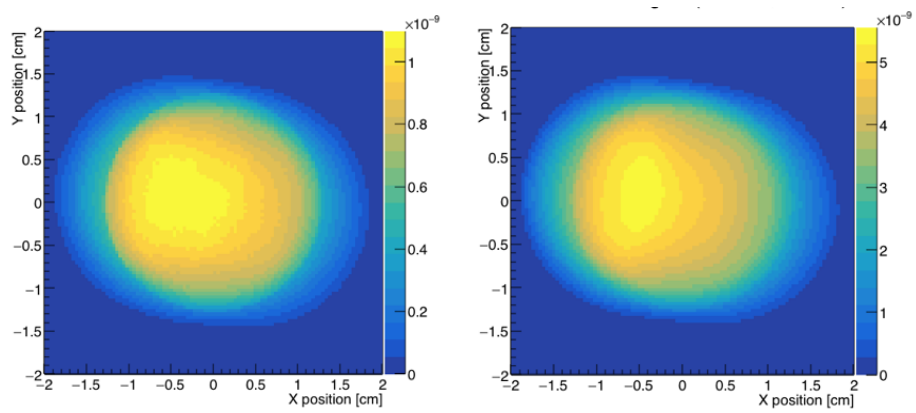

Figure 12: The spatial distribution of neutrons incident upon the upstream actinide target in the fissionTPC, as determined by the MCNP model of the 90L beam line: (left) E_n =100 keV and (right) E_n =10 MeV. The nonuniformity is a result of the choice of collimator design which creates a pinhole camera effect. Note the change in the shape along the x-axis is parallel to the direction of the proton beam incident on the spallation target.

The overlap term arises in recognition that a given shape of target and beam intensities, while the same in aggregate to a different shape, may result in differing rates of induced fissions. For example, if the most intense regions of the beam and target coincide, the fission rate is enhanced relative to the case where the beam and target intensities are anti-correlated. If this overlap term is not corrected, the result is a systematic shift in the measured (n,f) cross section.

Because the fissionTPC can reconstruct α and fission fragment starting vertices, the nonuniformity of both the beam and target can be characterized, and the overlap term corrected. Alternatively, the beam shape can be calculated, as described above, though there is no similar method for calculating the target shape, apart from simply assuming any given distribution. The overlap term is motivated by the well-known equation describing the fission rate:

$$f = \sigma n L \frac{T}{V} \tag{1}$$

where σ is the interaction cross-section, n is the neutron flux, L is the depth of the target, T is

the number of target nuclei, and V is the volume. The ratio T/V is simply the number density of the target actinide, and is therefore a physical constant. The term LT/V is therefore the areal density of the target, which itself can vary over the extent of the target. Because the overlap term is meant to be a normalized correction factor, the constants of the term drop out, and normalizations are applied to ensure the n and T terms by themselves do not change the overall cross-section measurement, but only their cross-terms. The resulting normalized equation is

$$\begin{aligned} \text{OT} &= \text{Overlap Term} \\ &= B \sum_i \frac{n_i}{\sum_j n_j} \frac{T_t}{\sum_k T_k} && (2) \\ &= B \frac{1}{\sum_j n_j} \frac{1}{\sum_k T_k} \sum_i n_i T_i && (3) \end{aligned}$$

In the the above equation the value B is the number of bins into which the data is divided. This term is necessary to remove the dependency of bin size on the final calculation. n_i is the number of neutrons traversing bin i in any given length of time, and T_i is the number of target nuclei in bin i. Note that in Eq. (2) the term is normalized by the total number of neutrons and the total number of target nuclei, to ensure that only the interplay between n_i and T_i are corrected in the final calculation. In Eq. (3) the normalizations, being constant, are brought outside the summation over i.

The summation over n_j is a measure of the total neutron beam, and can be obtained in multiple ways. One way is via Monte Carlo calculation, as shown in Fig. 12. Another approach is referred to as the "self-calibrating" method, where the shape of the target, given by the α start vertices, is used to infer the beam shape from the distribution of fission fragment starting vertices from the same target. We point out, however, that once known, the beam shape can be applied to any *in situ* beam target, allowing us to determine the beam shape from one target and apply it to a second target in the same beam. The mathematics governing these different approaches are explored later in this section.

Eq. (3) can be recast in terms of the experimental observables f_i, the number of fission fragments detected in bin i in a given length of time, and α_i, the number of alpha particles detected over that same length of time in the same bin:

$$\begin{aligned} f_i &= \sigma n_i L_i \frac{T}{V} \\ \Rightarrow n_i &= \frac{1}{\sigma} \frac{f_i}{L_i} \frac{1}{\rho} && (4) \end{aligned}$$

where the ratio T/V has been replaced by the constant ρ. In a similar vein, the number of target nuclei in any given bin can be related to the thickness of the target in that location:

$$T_i = \rho L_i A_{bin} \tag{5}$$

where A_{bin} is the area of bin i. Substituting Eqs. (4) and (5) into Eq. (3) gives

$$\mathrm{OT} = \frac{1}{\frac{1}{\sigma\rho}\sum_j \frac{f_j}{L_j}} \frac{1}{\rho A_{bin} \sum_k L_k} B \sum_i \frac{1}{\sigma}\frac{f_i}{L_i}\frac{1}{\rho}\rho L_i A_{bin} \tag{6}$$

$$= \frac{1}{\sum_j \frac{f_j}{L_j}} \frac{1}{\sum_k L_k} B \sum_i f_i \tag{7}$$

Note that the terms σ, ρ, and A_{bin} have all cancelled, leaving behind a term purely governed by the shapes of the target and beam.

L_i can be defined in terms of the rate from any given region of the target via

$$\begin{aligned} R_i &= \text{alpha rate in bin } i \\ &= \frac{dT}{dt}|_{t=0} = \frac{ln2}{\tau_{1/2}} T_{0_i} \\ &= \frac{ln2}{\tau_{1/2}} \rho L_i A_{bin} \\ \Rightarrow L_i &= \frac{\tau_{1/2}}{ln2} \frac{1}{\rho A_{bin}} R_i \end{aligned} \tag{8}$$

By recognizing that $R_i = t\ \alpha_i$, where t is the length of time over which data is acquired, Eq. (8) can be substituted into Eq. (6) to give

$$\mathrm{OT} = B \left[\sum_j \frac{f_j}{\alpha_j} \frac{\sum_k \alpha_k}{\sum_i f_i} \right]^{-1} \tag{9}$$

Depending on the method used to determine the beam shape, we may want to work either in simulation space, where the independent observables are the n_i and T_i, or experimental space, where the independent variables are f_i and α_i. In the former case, we employ Eq. (3), while in the latter we use Eq (9). We also have the option of transforming our independent terms according to the equations

$$T_i = \frac{\tau_{1/2}}{t\ ln2} \alpha_i \tag{10}$$

$$n_i = \frac{A_{bin}}{\sigma} \frac{t\ ln2}{\tau_{1/2}} \frac{f_i}{a_i} \tag{11}$$

Even though terms such as $\tau_{1/2}$ and σ that are specific to any given actinide are present in these equations, in practice they tend to cancel when calculating a ratio of overlap terms. As an example, we examine the case where the target (T_i) terms are taken from a plutonium target, but the beam terms (n_i) are taken from a correlated uranium target. Beginning with Eq. (3) we derive:

$$\begin{aligned} \mathrm{OT}^{Pu} &= B \frac{1}{\sum_j n_j^U} \frac{1}{\sum_k T_k^{Pu}} \sum_i n_i^U T_i^{Pu} \\ &= \frac{1}{\sum_k \alpha_k^{Pu}} \frac{1}{\sum_i \frac{f_i^U}{\alpha_i^U}} \sum_j \frac{f_j^U}{\alpha_j^U} \alpha_j^{Pu} \end{aligned} \tag{12}$$

where the superscripts are used to denote the nature of the experimental target that are used to originate the term. This OT^{Pu} term is described as the "uranium-corrected plutonium overlap term". As previously mentioned, this plutonium overlap term can be self-corrected (if the reader prefers, "plutonium-corrected plutonium overlap term"), or corrected by the Monte Carlo calculations ("MCNP-corrected plutonium overlap term"). A ratio of OT^{Pu} / OT^{U} will have the sum over i cancel, and in the OT^{U} term the α terms in the sum over j will also cancel. This leaves the final ratio as

$$\frac{\mathrm{OT}^{Pu}}{\mathrm{OT}^{U}} = \frac{\frac{1}{\sum_k \alpha_k^{Pu}} \sum_j \frac{f_j^u}{\alpha_j^U} \alpha_j^{Pu}}{\frac{1}{\sum_i \alpha_i^U} \sum_l f_l^U} \tag{13}$$

where again, the physical constants and non-experimental terms have cancelled, leaving a purely shape-dependent expression for the overlap term.

Because the beam is largely stable from run to run, by rotating the target within the beam, the overlap term can be made to change. This stems from a region of greater or lesser target density being inserted into a region of greater or lesser neutron beam flux. The result of such a rotation is shown in Fig. 13.

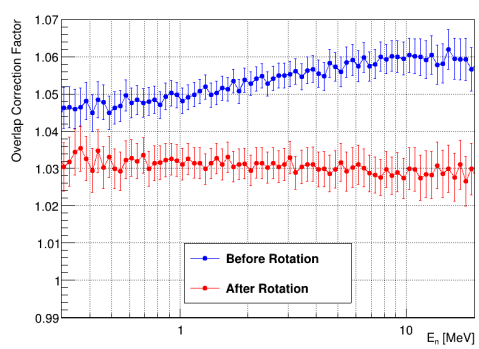

Figure 13: The overlap correction for "Before" and "After" rotation of the fissionTPC. The two orientations were 180° about the vertical axis with respect to the beam direction, which had the effect of reversing the beam and target maxima with respect to each other.

3.2 The Binned Analysis

The binned analysis bypasses the need for an overlap correction by taking a back-to-back cross section ratio in each spatial bin such that the bin size is small enough that the beam and/or target is relatively uniform over the bin size. The target-atom ratio has to be scaled for each bin using the α-decay data. The total cross section is then determined by averaging each binned cross section result. One has to take care in how the averaging is done. The arithmetic mean is the incorrect choice for averaging ratios as

$$\langle \sigma_0/\sigma_1 \rangle \neq \langle \sigma_0 \rangle / \langle \sigma_1 \rangle \tag{14}$$

where the subscripts 0 and 1 refer to the back-to-back targets. A geometric mean $\left(\Pi_{i=1}^{N} r_i\right)^{1/N}$ is the appropriate operation for averaging ratios, which respects taking the inverse. We can switch between arithmetic and geometric mean formulations using logarithms and exponentials

$$e^{\sum \ln r_i} = \Pi r_i. \tag{15}$$

The generic weighted geometric average formulation is then

$$\ln \frac{\sigma_0}{\sigma_1} = \frac{\int w(x) \ln \frac{F_0(x)\rho_1(x)}{F_1(x)\rho_0(x)} d\mathbf{x}}{\int w(x) d\mathbf{x}}, \tag{16}$$

where $w(x)$ is a weight, $F_v(x)$ are the fission fragment counts and $\rho_v(x)$ are the target atom densities all with spatial coordinate x. The target atom density $\rho_v(x)$ is proportional to the autoradiograph alpha counts $\alpha_v(x)$ where the proportionality constant is determined from the atom number counting measurements. The weight was chosen such that bins with the lowest uncertainty will have the highest weight. The main uncertainty that varies between bins is the counting statistics of the fragment F_v and alpha counts α_v. The statistical uncertainty on a particular bin due to counting fluctuations in F_0 for example is $\partial F_0 = \sqrt{F_0}$ is

$$\delta^2_{F_0} = \left(\partial F_0 \frac{\partial}{\partial F_0} \ln \frac{F_0 \rho_1}{F_1 \rho_0} \right)^2 = \left(\frac{\partial F_0}{F_0} \right)^2 = \frac{1}{F_0}. \tag{17}$$

The uncertainty is likewise for other components. The total statistical variance is the sum of the independent counting variances and the weight for each bin is $1/\delta^2$, thus

$$\delta^2 = \frac{1}{F_0} + \frac{1}{F_1} + \frac{1}{\alpha_0} + \frac{1}{\alpha_1} \tag{18}$$

and

$$w(x) = \frac{1}{\frac{1}{F_0} + \frac{1}{F_1} + \frac{1}{\alpha_0} + \frac{1}{\alpha_1}}. \tag{19}$$

The treatment above assumes our binning discretization leaves plenty of counts for F_v and α_v in each bin, above where we need to worry about small-number fluctuations. The weighting function in Eq. 19 assigns a weight of zero to any bins with zero counts in any category. It does, however, introduce some systematic bias to the answer due to being correlated with the counts in the ratio.

The residuals between the cross section result when applying the overlap correction and when using the binned analysis are shown in Figure 14. A residual of zero across all energy bins indicates that the results of the two methods are consistent. Figure 14 represents a cross-validation for the two methods of addressing the beam and target nonuniformity.

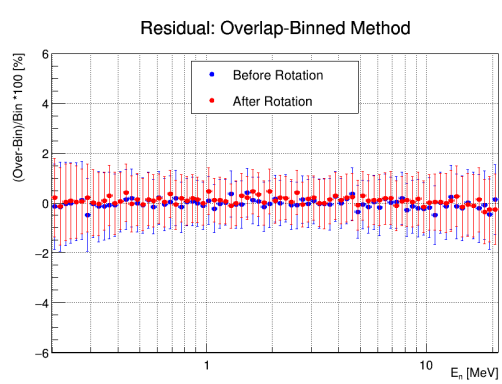

Figure 14: The residual between the cross section results using the overlap correction compared to using the binned analysis for the two orientations of the fissionTPC. The results of the two methods are consistent. The error bars are statistical only for the binned analysis.

Applying an overlap correction is the preferred method for calculating a final cross section result as it is not subject to increased uncertainties from binning the fission fragment statistics and is not subject to the weighting bias in the binned analysis. The effects of the weighting bias can be seen in Figure 15. The results were found to be stable over a wide range of bin sizes from 0.64 mm^2 (square bins 0.8 mm on a side) to 4.0 mm^2, wherein the statistics are sufficiently high and the beam is relatively uniform. Below 0.64 mm^2 bin size a bias at high and low energy can be seen. The bias at these energies is a result of the decreasing cross section ratio and low fission statistics. Above 4.0 mm^2 bin size the results are shifted systematically across all energy bins which is to be expected as the beam is no longer uniform over the bin.

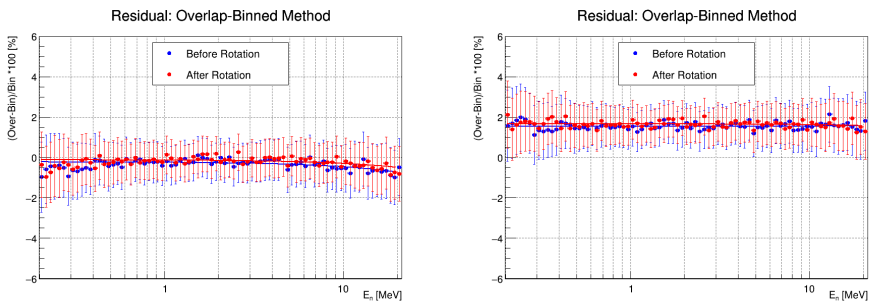

Figure 15: The Overlap-Binned residual for different bin sizes used in the binned analysis. The residual for bin sizes of 0.36 mm^2 (left) and 16.0 mm^2 (right) are shown in the figure to illustrate the bias at small bin size and the systematic shift at large bin size. A 1st order polynomial fit is shown to further illustrate the effect. The bias at small bin size is a result of low statistics while the shift at large bins is a result of the beam no longer being uniform over the bin width. The results are stable between a bin size of approximately 0.64 mm^2 and 4 mm^2.

3.3 Cross Section Shape Validations and Sensitivity Studies

3.3.1 Rotation

The primary validation for the fissionTPC analysis is the rotation validation. The detector was rotated 180° about the vertical axis in the beam line. The rotation flipped the targets with respect to being upstream or downstream of the beam. The rotation acts as a validation for the efficiency model which is sensitive to the angular distribution of the fission fragments. The angular distribution is driven in large part by the kinematic boost of the incident neutrons which is sensitive to the direction of the actinide and backing with respect to the beam direction. Figure 16 shows the fission fragment detection efficiency for the two targets in both orientations of the fissionTPC. The change in detection efficiency with rotation is significant, approaching 4% at 20 MeV incident neutron energy.

Figure 17 shows the residual between the measured cross section for before and after rotation (BR and AR). The residual is shown for both the overlap corrected and binned analyses. A 1st order polynomial fit of the data is shown for illustrative purposes. Generally the residual is consistent with zero. The fit indicates there may be a slight bias approaching 20 MeV, although the scatter in the data and the size of the error bars do not significantly support a bias. The current iteration of the efficiency model includes the use of FREYA, which our analysis indicates underestimates the energy given to the fission neutrons beginning at second chance fission. Furthermore FREYA is not expected to be accurate above 20 MeV. Our efficiency model is not dependent on

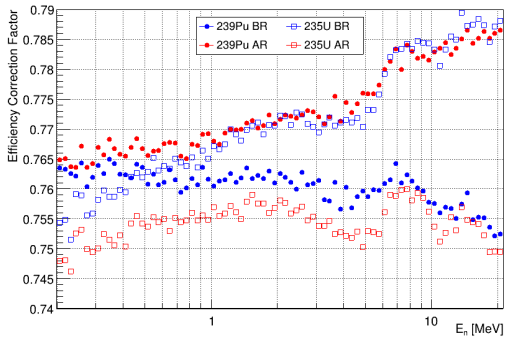

Figure 16: The calculated fission fragment detection efficiency of the fissionTPC. The detection efficiency in this plot is lower than the absolute detection efficiency because energy and angular cuts are taken into account. For a given orientation of the detector the fission fragments are either kinematically boosted into or away from the thick Aluminum backing, resulting in a large change in detection efficiency. BR and AR in the legend refer to before and after rotation. Also apparent in the plot is the quantum anisotropy introduced near 7 MeV or second chance fission.

FREYA, which was used only as an additional validation of the efficiency model. In the coming year we will explore the effects of the use of FREYA on any possible bias in the BR and AR analysis. A final cross section result would be the weighted average of the two rotation data sets which will average out any remaining bias not fully captured by the efficiency model.

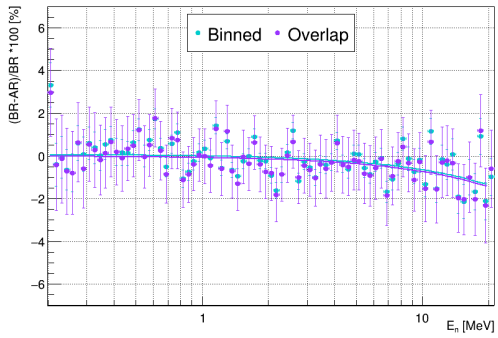

Figure 17: The residual between the measured cross section for before and after rotation, for both the overlap correction and binned analysis. A 1st order polynomial fit of the data is shown for illustrative purposes. The residual is consistent with zero within the error bars and scatter.

3.3.2 Radius Cut

The rotation also acts as an additional validation of the overlap correction as it flipped the region of greater or lesser ^{239}Pu target density being inserted into a region of greater or lesser neutron beam flux and had a significant impact on the overlap calculation as shown in Figure 13. In addition to the rotation validation an analysis was conducted making several radius cuts on the target. A radius cut has a large impact on the overlap calculation as the edge of the target represents a significant area of the target and also behaves as a large nonuniformity. Figure 18 shows the change in the magnitude of the overlap correction when cutting out the edge of the target. The overlap term moves by nearly 5% with a cut at 0.9 cm radius which is a reduction of 10% of the full

1 cm radius. Figure 19 shows the results for three radius cuts. The residual between the overlap correction based analysis and the binned analysis is shown along with the rotation residual for the overlap correction analysis. The results are stable with radius cut and do not change from those shown in Figures 14 and 17.

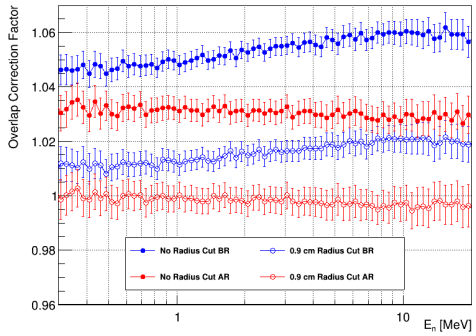

Figure 18: The overlap correction for BR and AR data sets and shown for two target radius cuts. The target is 1 cm in diameter. A cut of 0.9 cm is inside the target edge. The magnitude of the overlap term changes significantly as the edge represents a large area of the target and can be interpreted as a large target nonuniformity.

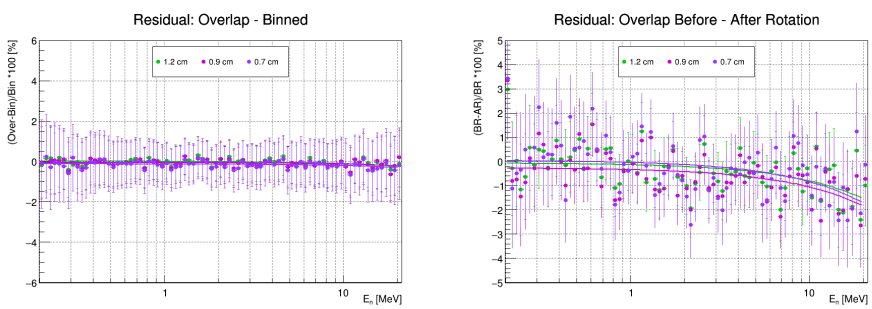

Figure 19: Residual plots for three different radius cuts: 1.2 cm encompasses the full target while 0.9 cm and 0.7 cm are within the targets 1 cm radius. (Left) The residual between the cross section results using the overlap correction compared to using the binned analysis for before rotation only. (Right) The residual between before and after rotation for the overlap-based analysis. These plots show that the cross section shape is stable with radius cuts.

In addition to acting as a validation for the overlap correction the radius cut acts as a validation of the vertex tracking in general. Not only are the overlap correction and binned analysis explicitly dependent on vertex tracking, but the overall mass ratio is significantly changed as a result of the large nonuniformity in the ^{239}Pu target. A cut of 0.9 cm radius (where the full target is 1 cm radius) results in an approximately 7% change in the target atom ratio which must be accounted for when calculating the cross section ratio. Figure 20 shows the residual between the cross section for each of the radius cuts (for BR and overlap correction only). The residual is consistent with zero which shows that not only is the shape stable, which is illustrated in Figure 19, but the normalization change is also properly accounted for by the α vertex tracking.

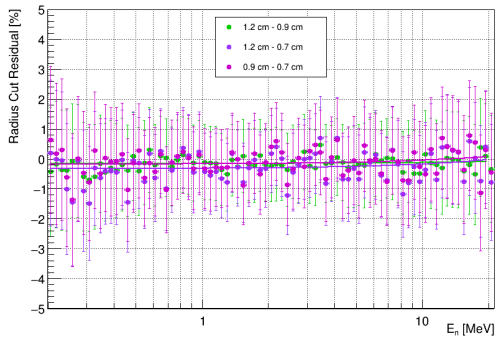

Figure 20: The residual between the cross section results for the three radius cuts. When applying a radius cut the overall target normalization must be adjusted as a result of the nonuniformity in the ^{239}Pu target. The zero residual is a validation of vertex tracking which must be used to adjust the target normalization.

3.3.3 Polar Angle, θ, Cut & Track Vertex Bias

The vertex tracking is subject to some bias resulting from the 2 mm pitch hexagonal pad structure of the anode. The tracking algorithm has a focusing procedure that on average eliminates the tracking bias, however in certain polar angle ranges the bias can become apparent. While the calculations for the overlap correction and binned analysis are done on the full polar angle range there is the potential for a systematic error from track vertex bias. A sensitivity study was performed on three track polar angle ranges that show the potential effects in the most extreme cases of the track biasing. Figure 21 shows the effects of track biasing on the ^{239}Pu target distribution, the hexagonal pattern is readily visible in two of the three polar angle ranges. Figure 22 shows the effect of the track vertex bias on the overlap correction and binned analysis. There is no change in the shape of the cross section, the residual between the overlap correction and the binned analysis is zero. The residual between cross sections resulting from the different biasing show the potential for a normalization shift of 0.5% in the most extreme case; the most extreme case being the difference between the cos(θ) ranges of 0.2–0.4 and 0.6–0.8 where the hexagonal biasing reverses from rings to points.

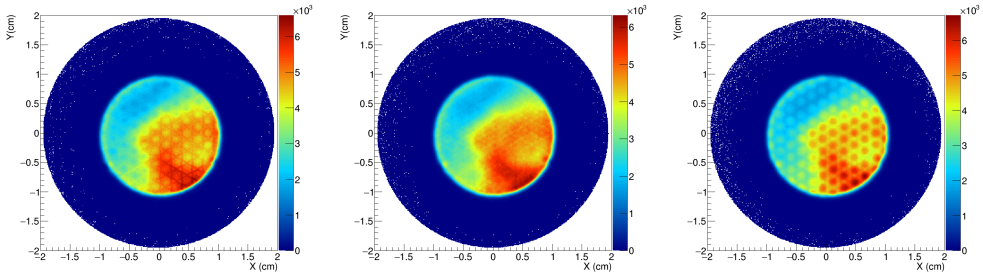

Figure 21: The tracking algorithm can bias vertices toward the edges or centers of the hexagonal anode pads of the fissionTPC. The algorithm is adjusted so that this effect is averaged out for all tracks but selecting a subset based on polar angle cuts can make the biasing apparent. The three plots show track vertices for cos(θ) cuts in the range of 0.2–0.4, 0.4–0.6, and 0.6–0.8 out of a full 2π range of 0–1.

The effect of track vertex biasing as a result of cos(θ) can be exaggerated by applying a radius

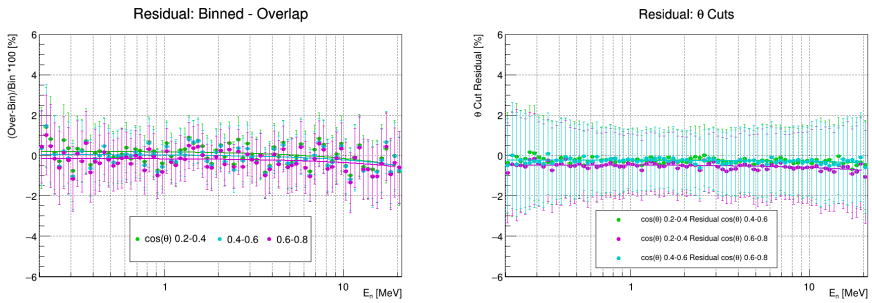

Figure 22: (Left) The residual between the cross section results using the overlap correction compared to the binned analysis for before rotation only. The zero residual indicates there is now shape change when applying a tracking bias (Right) The residual between the cross section results for the three cos(θ) cuts using the overlap correction (BR Only). The residual shows the potential for a 0.5% normalization bias in the most extreme case of vertex biasing.

cut in addition. Figure 23 shows the residual between different overlap correction-based cross section measurements using different track bias inducing cos(θ) cuts and a 0.9 cm radius cut. This can be compared to the right side of Figure 22 which had no radius cut. The radius cut combined with the angle cut shows a potential normalization bias of up to 1.5%. This shift however is almost entirely a result of the target-atom renormalization and not a change in the magnitude of the overlap correction. This can be understood if one visualizes a ring representing the radius cut which is then intersecting with the maxima and minima of the hexagonal grid pattern in an irregular fashion, resulting in a bias in how many tracks fall in and out of the radius cut.

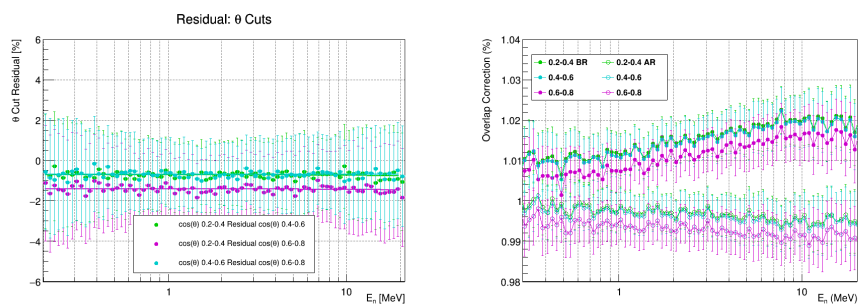

Figure 23: (Right) The residual between the cross section results using the overlap correction for the three cos(θ) cuts and a 0.9 cm radius cut (BR Only). The residual shows the potential for a 1.5% normalization bias in the most extreme case of vertex biasing. This shift is a result of the target ratio renormalization procedure and not a change in the magnitude of the overlap correction shift as evidenced by the magnitude of the overlap correction (Right) which moves by $<$0.5% for the most extreme biasing case.

The polar angle cut or track vertex biasing sensitivity study shows that the shape of the cross section is robust against track biasing that results from the hexagonal pad layout of the fissionTPC anode. There is however some potential for an overall normalization bias that must be accounted for in our uncertainty analysis. This uncertainty is likely less than 0.5%. While this is less than the 1.5% bias seen for the example of a radius and polar angle cuts shown in Figure 23, that figure should be interpreted in the context of the results from section 3.3.2 which discussed the radius cut sensitivity study. The stability of the result both in *shape and normalization* when performing radius cuts should be interpreted not only as a validation of the overlap correction but the accuracy of

the vertex tracking which is being used to correct for target normalization changes of greater than 5% to an accuracy much better than 1% (see Figure 20). While there is a dependence between track vertexing and track angle, the tracking algorithm's focusing setting is effectively averaging out the bias. Any remaining uncertainty from the track biasing would result in an overall cross section normalization uncertainty and be negligible for the shape uncertainty as evidenced by Figures 22 and 23.

3.3.4 Target Alignment

Another potential source of systematic error is the alignment between the two volumes of the fissionTPC. While the anode pad planes are precisely constructed printed circuit boards and are identical from one volume to the other, their alignment is not necessarily perfect as a result of the way the fissionTPC is assembled. The anodes are held in place by dowel rods that have approximately 200 μm of play. This means that the coordinate system from one volume is not necessarily aligned with the other, which would have an obvious impact on the overlap correction and binned analysis. The misalignment is corrected for by observing beam induced α tracks that have enough energy to pass through the cathode plane and deposit energy in both volumes. By observing the offset of the track vertices where they should intersect the alignment correction can be determined. The alignment correction to be applied to volume 1 was found to be -167 μm along the x-axis and -131 μm along the y-axis, well within the expected 200 μm maximum.

To understand the potential impact of an inaccurate alignment measurement a sensitivity study was conducted with the track vertices for both the α and fission fragment tracks being shifted by 200μm in one volume with respect to the other. The shift for fragments and αs were synchronized however as the data sets for target radiograph and cross section were taken without a disassembly of the fissionTPC in between. Figures 24 and 25 show the results. The cross section shape is stable with respect to the shift. A systematic normalization shift of approximately 0.5% between the overlap correction and the binned analysis was observed for some of the shifts. Similar results were shown for the residual between different shifts for an overlap correction-based cross section. This sensitivity study is the worst case potential misalignment for the data. Using the high energy α punch-through analysis for the volume alignment, we expect the cross section uncertainty from a target alignment uncertainty to be negligible for the shape and less than 0.5% for the normalization.

3.3.5 Space Charge Scaling

The high α-decay activity of the ^{239}Pu target results in a sustained space-charge of positive ions drifting towards the cathode in the fissionTPC drift volume. The space-charge causes a distortion in the drift field and the start vertices of the fission fragment and α distributions are drawn towards the center of the fissionTPC. The distortion produces a target distribution that appears smaller in the data than the target is in reality. Using an analysis of a photograph of the target, the ^{239}Pu data can be corrected by scaling the track vertices out radially. The correction was approximately 2% of the total radius. The size of the target and location of track vertices has obvious implications for the overlap correction and binned analysis as has been discussed throughout the previous sections. For a sensitivity study the space-charge correction was simply turned off. The space-charge correction has a 1.5% effect on the cross section normalization and no effect on the shape. This effect on normalization only occurs for an analysis of the entire target. When a radial cut is applied the normalization effect is no longer present. This can be understood in the way the overlap correction is calculated (see Section 3.1). The space-charge scaling has no effect on the beam size,

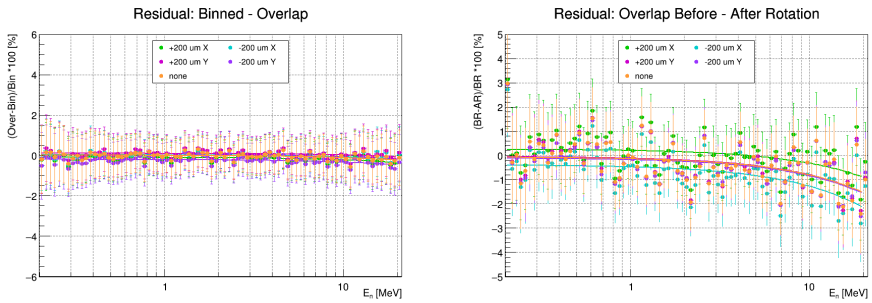

Figure 24: Residual plots for 4 different shifts of the target volumes with respect to each other, compared to the nominal alignment. (Left) The residual between the cross section results using the overlap correction compared to using the binned analysis for before rotation only. (Right) The residual between before and after rotation for the overlap-based analysis. These plots show that the cross section shape is stable with target shifts, with less than a 0.5% systematic disagreement introduced between the overlap and binned analysis for some shifts.

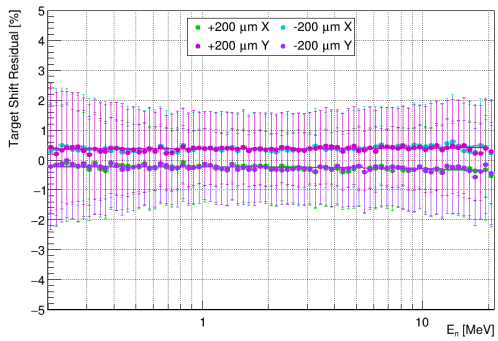

Figure 25: The residual between the cross section results (overlap correction, BR only) for 4 different shifts compared to the nominal alignment. The shape is stable with up to a 0.5% normalization systematic shift.

the scaling effectively changes the amount of area, and therefore the total number of neutrons, the target is exposed to. The correction does not change the number of target atoms, only the apparent density of the target. The overlap calculation normalizes the target distribution within whatever the cut radius is, therefore when a cut radius inside the scaling correction is applied the general shape of the target is largely unaffected and the target density is unchanged. In other words, turning off the space-charge scaling correction breaks the radial cut stability described in Section 3.3.2 and illustrated in Figure 26. This is a validation that the space-charge scaling correction is needed and being applied correctly. The uncertainty in the space-charge correction is a normalization uncertainty and has a negligible effect on the cross section shape.

3.3.6 Tracking Resolution

The overlap correction is sensitive the the interaction between the beam and the target edge as evidenced by the large change in the overlap correction with radius cuts (see Figure 18). The tracking resolution could produce a systematic error in the overlap correction. The tracking resolution was determined by fitting the edge of the target plotted in radial coordinates and was found to be 200 μm for fission fragments and 300 μm for α tracks. The different resolution of the two particle

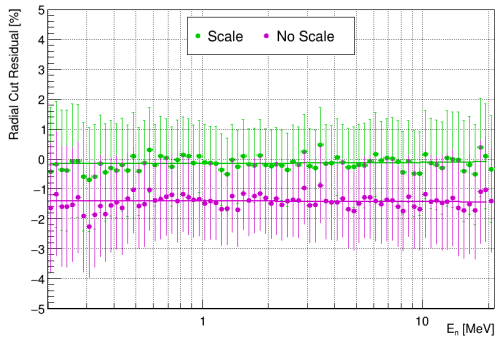

Figure 26: The residual between the cross section results for no radius cut and a 0.9 cm radius cut, with the space-charge scaling correction turned on and off (overlap correction, BR only). The shape is stable. When the scaling is turned off however the stability of the normalization for radius cuts is broken.

types is related to the charge cloud diffusion. The much greater charge deposited by a fission fragment results in a larger charge cloud that is less subject to vertex biasing induced by the pad plane pixels. The overlap correction was calculated using track vertex square bins ranging from 0.2 mm to 2.4 mm on a side, the results are shown in Figure 27.

The overlap term is stable up to a bin size of 0.8 mm with a 0.1% systematic shift at a bin size of 1.2 mm. At a bin size of 2.4 mm there is a 1% systematic shift in the overlap correction. The fact that the overlap correction is stable to 0.8 mm and has only a 0.1% shift at 1.2 mm, or 4 times the size of the tracking resolution, is a good indication that the resolution is sufficient to calculate the overlap correction for the edge of the target. Furthermore a change in the overlap correction with bin size is not unexpected as eventually the bin size will approach the size of the nonuniformities, and it is in fact encouraging that the shape is so stable. Figure 28 shows the ^{239}Pu target shape at a 0.4 mm and 1.2 mm bin size. Any uncertainty from tracking resolution appears as a normalization uncertainty and has a negligible effect on the cross section shape. When a radius cut is applied the overlap correction has only 0.1% shift at 2.4 mm bin size, further supporting the assertion that the uncertainty is entirely in the normalization.

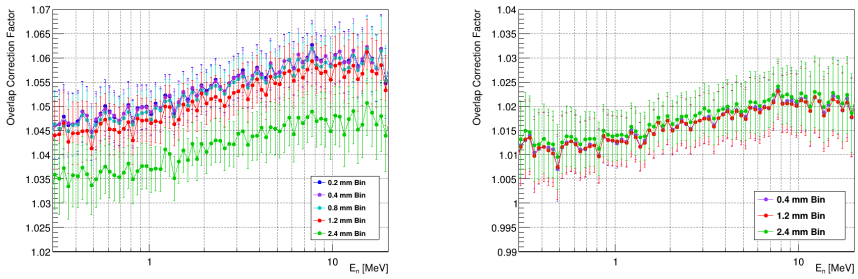

Figure 27: The overlap correction for various track vertex histogram bin sizes with two radius cuts. Any changes with bin size appear as an overall normalization shift and have no effect on the cross section shape. With no radius cut (Left) a shift of 1% is seen with a 2.4 mm square bin size. A shift in the overlap correction is to be expected as the bins become larger as the information about the target edge is being lost. With a radius cut of 0.9 mm (Right) the overlap correction is stable even through the 2.4 mm bin size as the edge no longer plays a role.

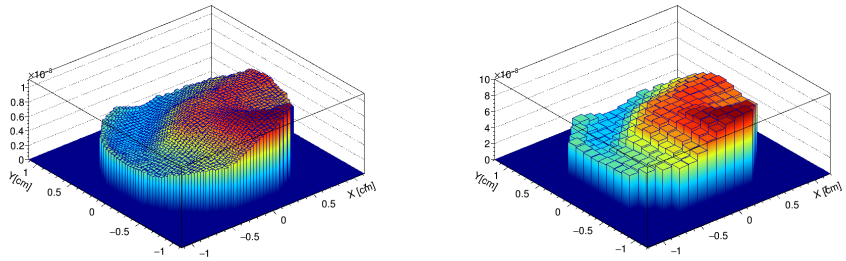

Figure 28: The ^{239}Pu target shape with a 0.4 mm bin size (Right) and a 1.2 mm bin size (Left). Information about the target edge begins to be obscured significantly at a bin size of 1.2 mm.

3.4 Cross Section Normalization

The target atom ratio normalization procedure is described in detail in the two previous NIFFTE cross section reports [3,4]. The targets were analyzed with mass spectrometry and α-counted both with a Silicon detector and the fissionTPC. The Si detector design was based on a NIST prescription for high precision counting. Because the target backing could be mounted with either actinide target facing the detector we were able to measure the target atom ratio directly to high precision without the need to account for the detector efficiency. The Si detector data collection and analysis took place in FY17. An independent analysis of the same data was conducted in FY18 and showed the same result $N_{235U}/N_{239Pu} = 1.742 \pm 0.006$. The fissionTPC analysis produced a result of 1.724 ± 0.021, which is in agreement with the Si detector measurement within the uncertainty reported. The results of the fissionTPC normalized cross section ratio compared to ENDF/B-VII.1 evaluation is shown in Figure 29.

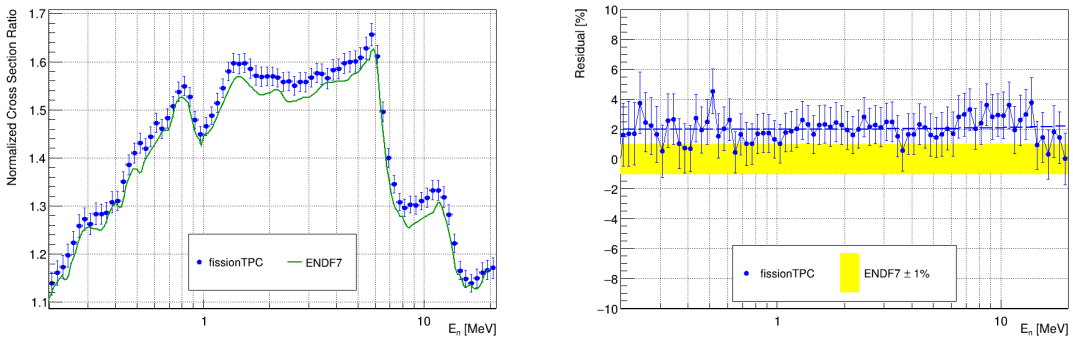

Figure 29: (Left) The normalized fissionTPC cross section ratio results shown with the ENDF/B-VII.1 evaluation. (Right) The residual between the ENDF and the fissionTPC results. The line is a 1st order polynomial fit to the data points and is for illustrative purposes only.

The results appear to be in good shape agreement with ENDF and approximately 2% systematically high on average. Figure 30 shows the fissionTPC results alongside those from References [11,12]. The Tovesson [11] measurement was on the same flight path (90L) at WNR-LANSCE that the fissionTPC data was collected on. The Lisowski [12] measurement was also measured at WNR-LANSCE, but on a different flight path. The Lisowski measurement was normalized with α-counting while the Tovesson measurement was normalized to the thermal cross section. Figure 31

shows the three measurements and the residual between the fissionTPC result and the Tovesson and Lisowski data. The results are largely in shape agreement at low energy and share many similar features when compared to ENDF/B-VII.1. The shape of all three measurements begin to diverge starting in the region of 10–20 MeV. It is interesting to note that the fissionTPC approach to detector efficiency is considerably different than in previous measurements, and its impact will be greatest at higher energy where kinematic boost and partial linear momentum transfer effects are at their greatest.

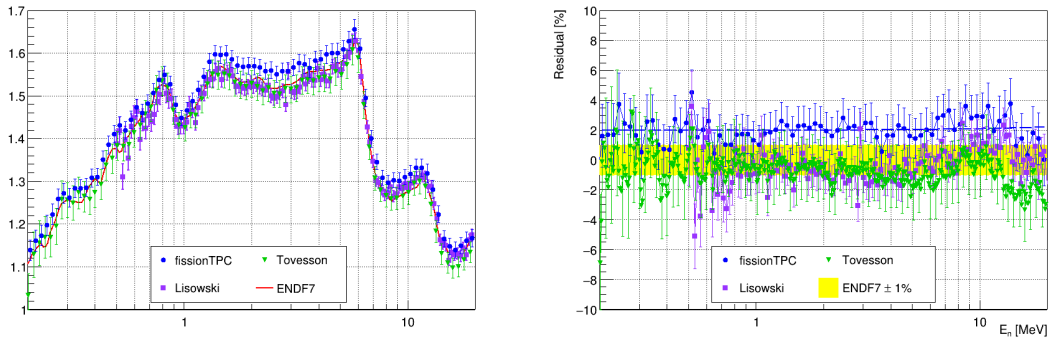

Figure 30: (Left) The normalized fissionTPC cross section ratio results and two other experimental results [11,12] shown with the ENDF/B-VII.1 evaluation. (Right) The residual between ENDF and the various data sets.

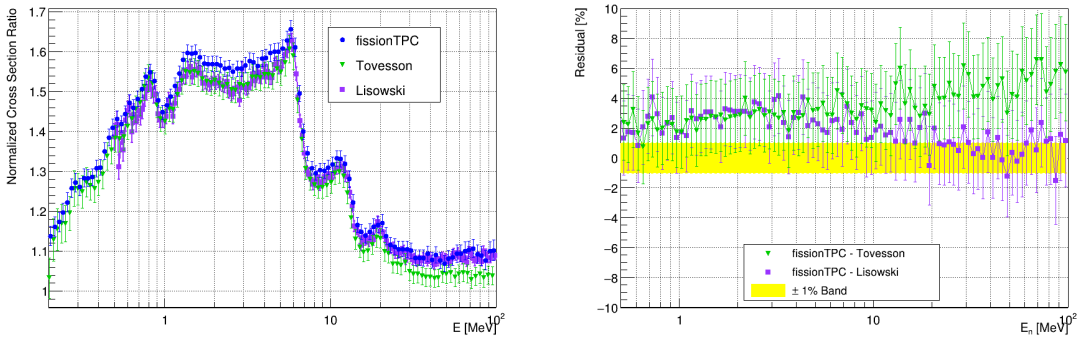

Figure 31: (Left) The normalized cross section ratio results from the fissionTPC, Tovesson [11], and Lisowski [12] for 0.2 – 100 MeV. (Right) The residual between the fissionTPC results and the Tovesson [11] and Lisowski [12] data.

While it is not the objective of the experiment to validate ENDF, and there is a need to be cautious of confirmation bias, the 2% systematic is well outside of the reported ENDF uncertainties. The fissionTPC results also appear to be systematically high when compared to the Tovesson measurement [11] which was made on the same beam line. While several of the sensitivity studies described in Section 3.3 indicate that we likely have a normalization error related to vertex tracking, none of those studies would indicate an error greater than 1%. This has led us to the conclusion that further analysis and measurement of the normalization is required. An additional normalization uncertainty will be determined based on the sensitivity studies reported here.

3.4.1 Summary

The large nonuniformity in the ^{239}Pu target combined with an energy dependent beam nonuniformity lead to the need for both normalization and energy-shape corrections. While these effects were anticipated prior to the measurement, and were estimated to be small, the magnitude of the target nonuniformity combined with a less than optimal beam-target alignment greatly exacerbated the effects. Fortunately the fissionTPC was designed specifically to understand the effects of such nonuniformities. The complexity of the data and the precision demands not only necessitated but allowed for an unprecedented and extensive validation effort (the NIFFTE reports include many studies not specifically referenced here [3,4]). While previous measurements made every effort to minimize nonuniformities and take advantage of the experimental arrangement of a ratio measurement (particularly for efficiency), it is likely that some unaccounted for systematic uncertainties were present. While the effects on nonuniformity were likely much larger in the fissionTPC data as compared to previous measurements, our ability to directly quantify and correct for them gives us great confidence in the shape measurement. Some questions remain over the normalization and will be addressed in the coming year. Currently an effort is underway to remeasure the target with the Silicon detector. Additionally, an extensive internal audit of the analysis is ongoing. Futhermore an effort is currently underway to produce a new ^{239}Pu target through the vapor deposition process, which will produce highly uniform targets. Lastly, LANL is producing a detailed model of the WNR beam lines and designing collimation for 90L to maximize beam uniformity.

[1] M. Heffner, et al. A time projection chamber for high accuracy and precision fission cross-section measurements. *Nuclear Instruments and Methods in Physics Research, Section A: Accelerators, Spectrometers, Detectors and Associated Equipment*, 759:50–64, 9 2014. `https://www.sciencedirect.com/science/article/pii/S0168900214005890?via%3Dihub`.

[2] R.J. Casperson, et al. Measurement of the normalized $^{238}\mathrm{U}(n,f)/^{235}\mathrm{U}(n,f)$ cross section ratio from threshold to 30 MeV with the NIFFTE fission Time Projection Chamber. *Phys. Rev. C*, 97:034618, Mar 2018. `https://link.aps.org/doi/10.1103/PhysRevC.97.034618`.

[3] NIFFTE Collaboration. Measurement of the ^{239}Pu(n,f)/^{235}U(n,f) Cross-Section Ratio from 200 keV to 30 MeV with the Fission Time Projection Chamber. Technical Report LLNL-TR-732603, Lawrence Livermore Natl. Lab.

[4] NIFFTE Collaboration. FissionTPC FY2018 Report. Technical Report LLNL-TR-758079, Lawrence Livermore Natl. Lab.

[5] D. Neudecker. Standard-like Evaluation using Mock-up Data for 239-Pu(n,f) relative to 6Li(n,a) and 1H(n,el). Technical Report LA-UR-18-31010, Los Alamos Natl. Lab.

[6] International Atomic Energy Agency. Neutron Cross-Section Standards, 2006. `https://www-nds.iaea.org/standards/codes.html`.

[7] A.D. Carlson, et al. Evaluation of the neutron data standards. *Nuclear Data Sheets*, (148):143–188, 2018.

[8] Georgios Giorginis and Vitali Khriatchkov. The effect of particle leaking and its implications for measurements of the (n,α) reaction on light elements by using ionisation chambers. *Nuclear Instruments and Methods in Physics Research Section A: Accelerators, Spectrometers, Detectors and Associated Equipment*, 538(1):550 – 558, 2005.

[9] R. Bencardino, R. Bevilacqua, G. Giorginis, and F.-J. Hambsch. Kinematics of the 6Li(n, t)4He Reaction and Experimental Scenarios for Cross-Section Measurement. *Nuclear Science and Engineering*, 177(1):68–76, 2014.

[10] L. Snyder, et al. Performance of a MICROMEGAS-based TPC in a high-energy neutron beam. *Nuclear Instruments and Methods in Physics Research Section A: Accelerators, Spectrometers, Detectors and Associated Equipment*, 881:1 – 8, 2018. `http://www.sciencedirect.com/science/article/pii/S0168900217310902`.

[11] F. Tovesson and T.S. Hill. Cross sections for ^{239}Pu(n,f) and ^{241}Pu(n,f) in the range E_n = 0.001 ev to 200 mev. *Nuclear Science and Engineering*, 165(2):224–231, 2010.

[12] P.W. Lisowski, J.L. Ullmann, S.J. Balestrini, A.D. Carlson, O.A. Wasson, and N.W Hill. Proc. int. conf. nuclear data for science and technology. page 97, Mito, Japan, 1988. Saikon Publishing Company Limited.